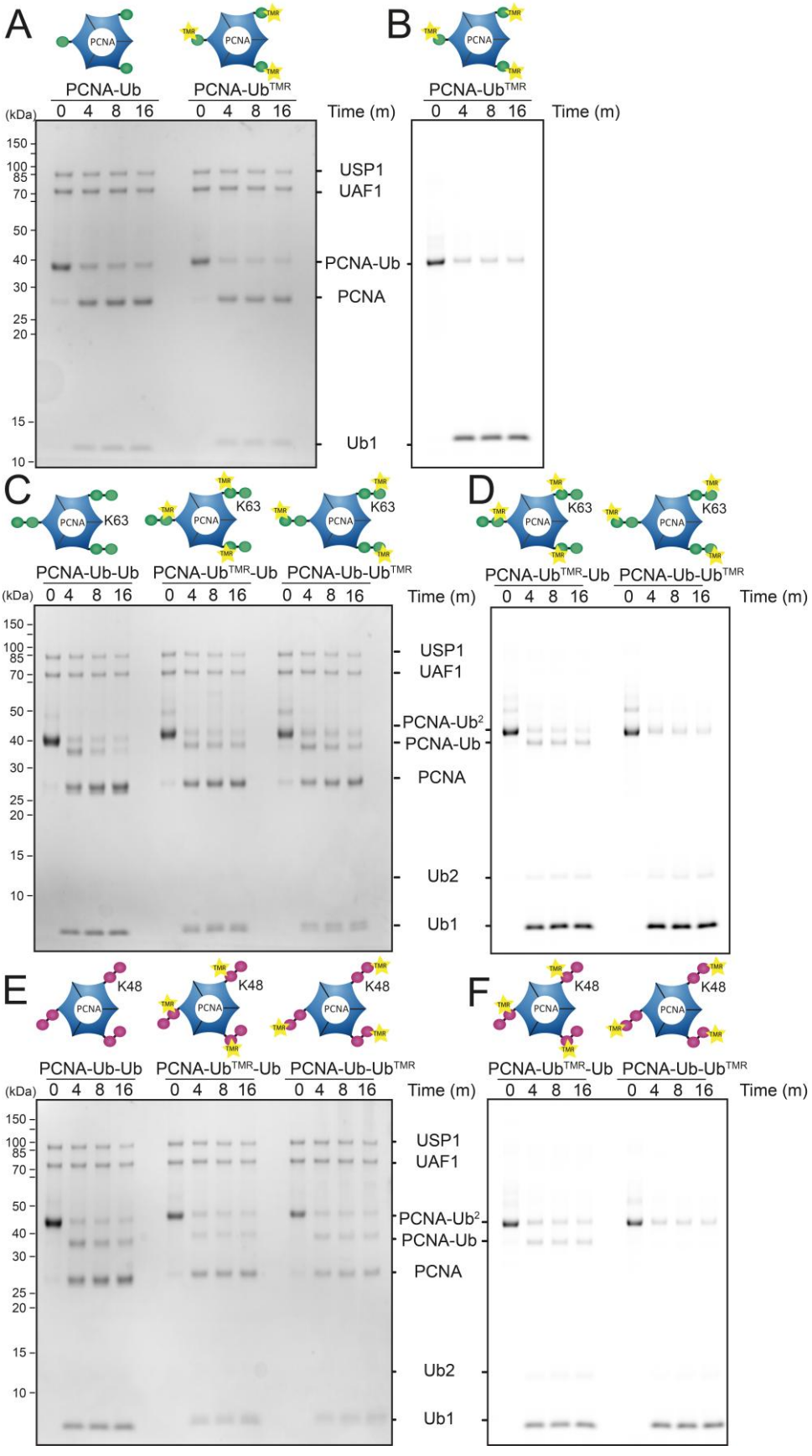

Supplementary figure 1 – A TAMRA label on residue 28 (A28C) of ubiquitin does not interfere with cleavage

A) DUB assay of USP1/UAF1 on PCNA-Ub and PCNA-Ub^{TMR}. Coomassie staining (left panel) shows that TMR-labeled Ub^{A28C} does not hinder deubiquitination by USP1/UAF1. **B)** Fluorescent scan of the PCNA-Ub^{TMR} DUB assay. **C)** DUB assay on K63-PCNA-Ub-Ub compared with K63-PCNA-Ub^{TMR}-Ub and K63-PCNA-Ub-Ub^{TMR} shows that the Ub^{A28C} label does not affect cleavage. **D)** Fluorescence image of gel shown in C. **E)** DUB assays on K48-PCNA-Ub-Ub compared with A28C labeled K48-PCNA-Ub^{TMR}-Ub and K48-PCNA-Ub-Ub^{TMR} shows that the label does not affect cleavage. **F)** Fluorescence image of gel shown in F. **ABCDEF)** Uncropped gels are provided in source data file.

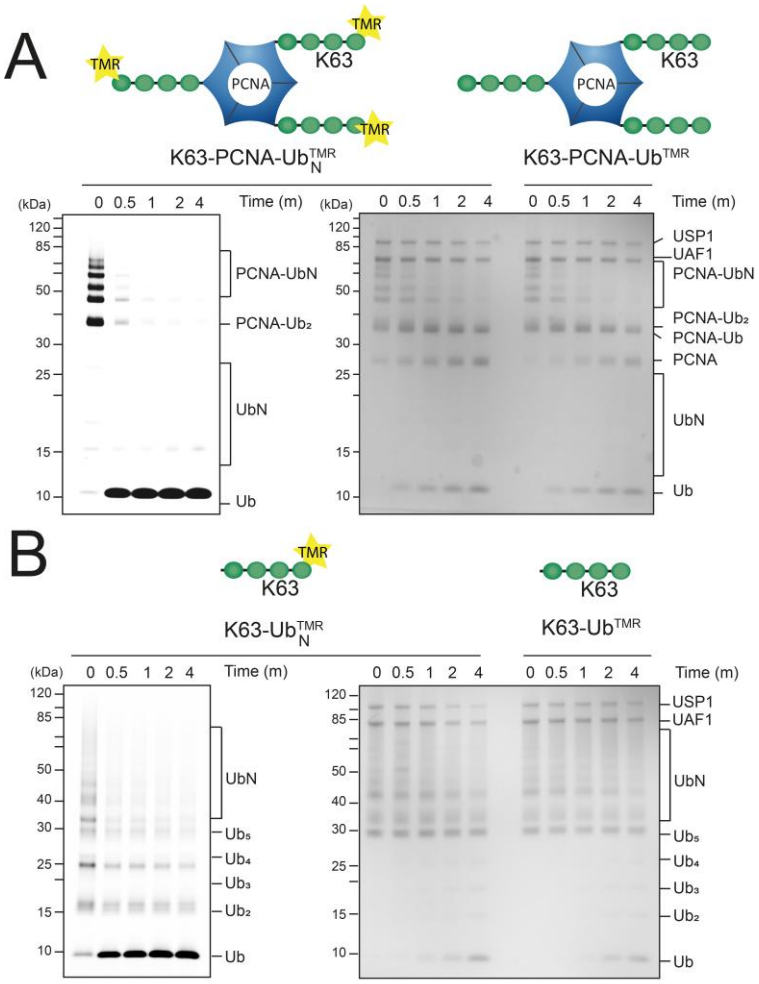

Supplementary figure 2 – USP1/UAF1 retains its strong exo-cleavage preference on longer ubiquitin chains

A) DUB assay using K63-PCNA-Ub_N, topped with a distal $Ub^{K63R\text{-}TMR}$. Fluorescent scan image demonstrates that all TMR-labeled ubiquitin is cleaved off as a single ubiquitin, verifying the strong exo-cleavage preference that was observed in the crosslinking experiment (Fig. 1). Uncropped gels are provided in source data file. **B)** DUB assay using unanchored K63-Ub_N, topped with a distal $Ub^{K63R\text{-}TMR}$, on which USP1/UAF1 demonstrates a preference for exo-cleavage as well, as only the single ubiquitin band increases over time. It is therefore the ubiquitin chain itself and not PCNA that causes USP1/UAF1 to prefer exo-cleavage. We used high exposure in the fluorescent image in order to be able to see TMR-labeled ubiquitin chains, leading to more visible background bands than in the coomassie stained gel. This is likely caused by long ubiquitin chains (+/- Ub6 and longer) not running well on SDS-page gels, appearing as a smear which dilutes the TMR signal. Uncropped gels are provided in source data file.

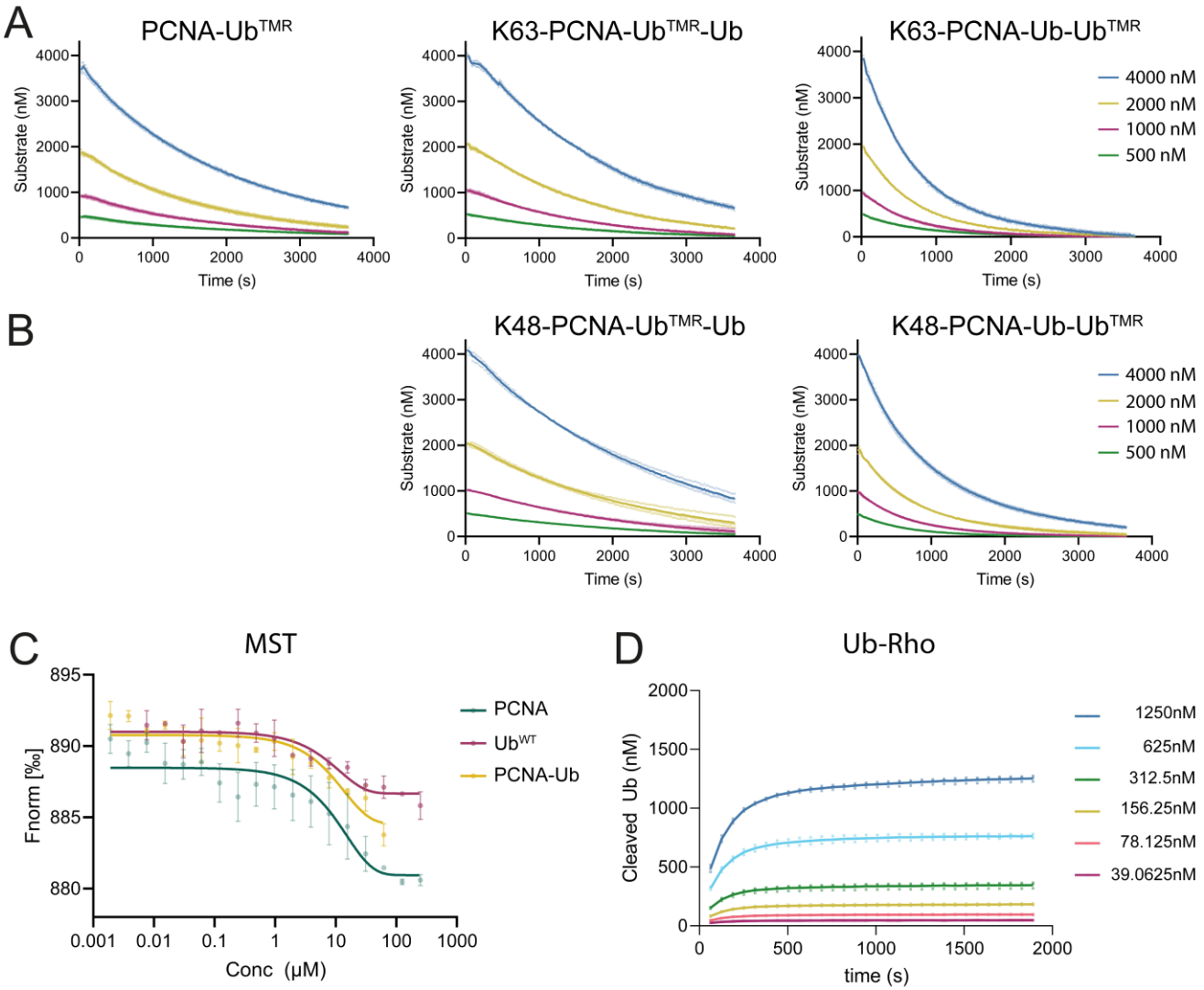

Supplementary figure 3 – Experimental data used for kinetic modeling

A) FP assays on PCNA-Ub^{TMR}, proximally and distally labeled K63-PCNA-Ub$_2$. A single concentration of USP1 (10 nM) was tested against four concentrations (4 µM, 2 µM, 1 µM, 0.5 µM) of labeled substrate. Coloured lines show average of three technical repeats (transparent dots). Source data (raw fluorescent anisotropy) are provided in the corresponding source data file. **B)** FP assays on proximally and distally labeled K48-PCNA-Ub$_2$. Coloured lines show average of three technical repeats (transparent dots). Source data is provided in corresponding source data file.**C)** Microscale Thermophoresis analysis of USP1^{WT}/UAF1^{WT} binding to PCNA-Ub^{L73P}, PCNA and ubiquitin. For this analysis, USP1/UAF1 was randomly labeled using DY-574P1-maleimide (methods). Soure data are provided. **D)** Ub^{Rho} fluorescence intensity assay that we published previously (Keijzer et al., 2024; Fig. S2A, upper left panel) was used to accurately determine K$_{cut}$ (cleavage) to support global kinetic analysis.

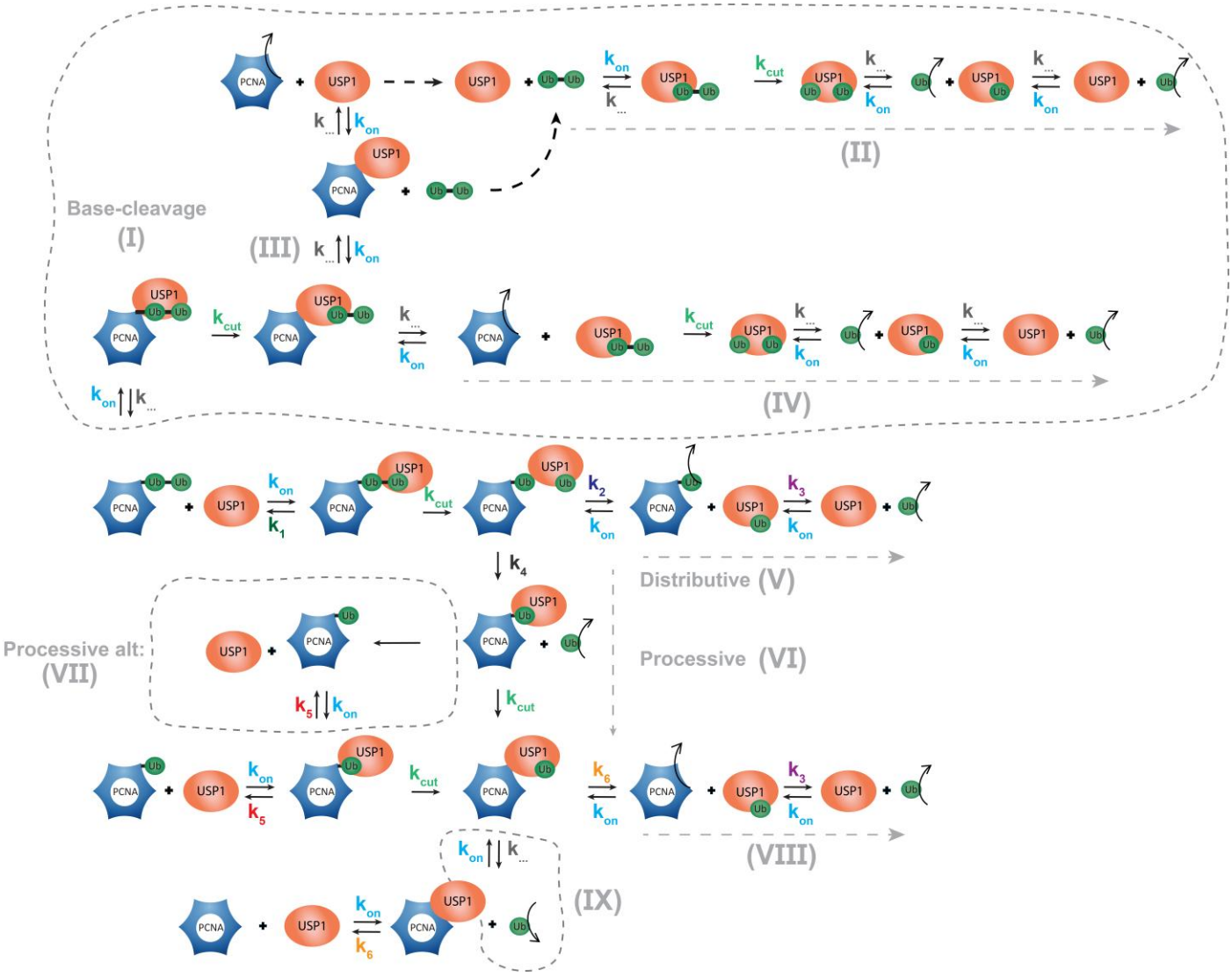

Supplementary figure 4 – Global kinetic model before optimization

In order to generate a kinetic model that fits our experimental data, we started by describing all possible steps that USP1 can take to cleave a PCNA-Ub_2. The process of generating the kinetic model was an iterative process: Many different combinations of reaction steps (indicated with roman numerals) were tested, upon which we evaluated whether the fit improved or worsened. Such a reaction step can refer to a single reaction constant, or a series of reaction constants. The components which were not used in the final kinetic model (Fig. 3B) are highlighted with a dashed line. It is important to emphasize that these were not the only components that were tested. Components that are included in the final model have been eliminated in certain stages of model development, but when this resulted in worsening of the fit they were reintroduced. For example, a model without distributive cleavage (V), or a model that only consisted of base-cleavage (I).

One component that was eliminated in the final model describes base-cleavage (I) and all steps involved. Within base-cleavage, different paths are possible. After base cleavage USP1 can hold on to Ub-Ub (IV), which it can then continue to cleave. However, after base-cleaving, USP1 can also release diubiquitin, remain bound to PCNA (III). When USP1 then releases from PCNA it can still bind and cleave the free diubiquitin chain (II). None of these options, and base-cleavage in general, improved the model.

In another component, two different variants of processive cleavage were written: The one used in the final model (Bind, cleave, cleave again (VI)), and an alternative processive model (Bind, cleave, release, bind PCNA-Ub and start cleavage (VII)). For a good fit of the model, it was essential that USP1 could not use the alternative processive model.

We also tested variants in which USP1, after mono-cleaving PCNA-Ub, releases ubiquitin and remains bound to PCNA (IX). However, the model in which USP1 remains bound to ubiquitin and releases PCNA (VIII) was more in accordance to our experimental data.

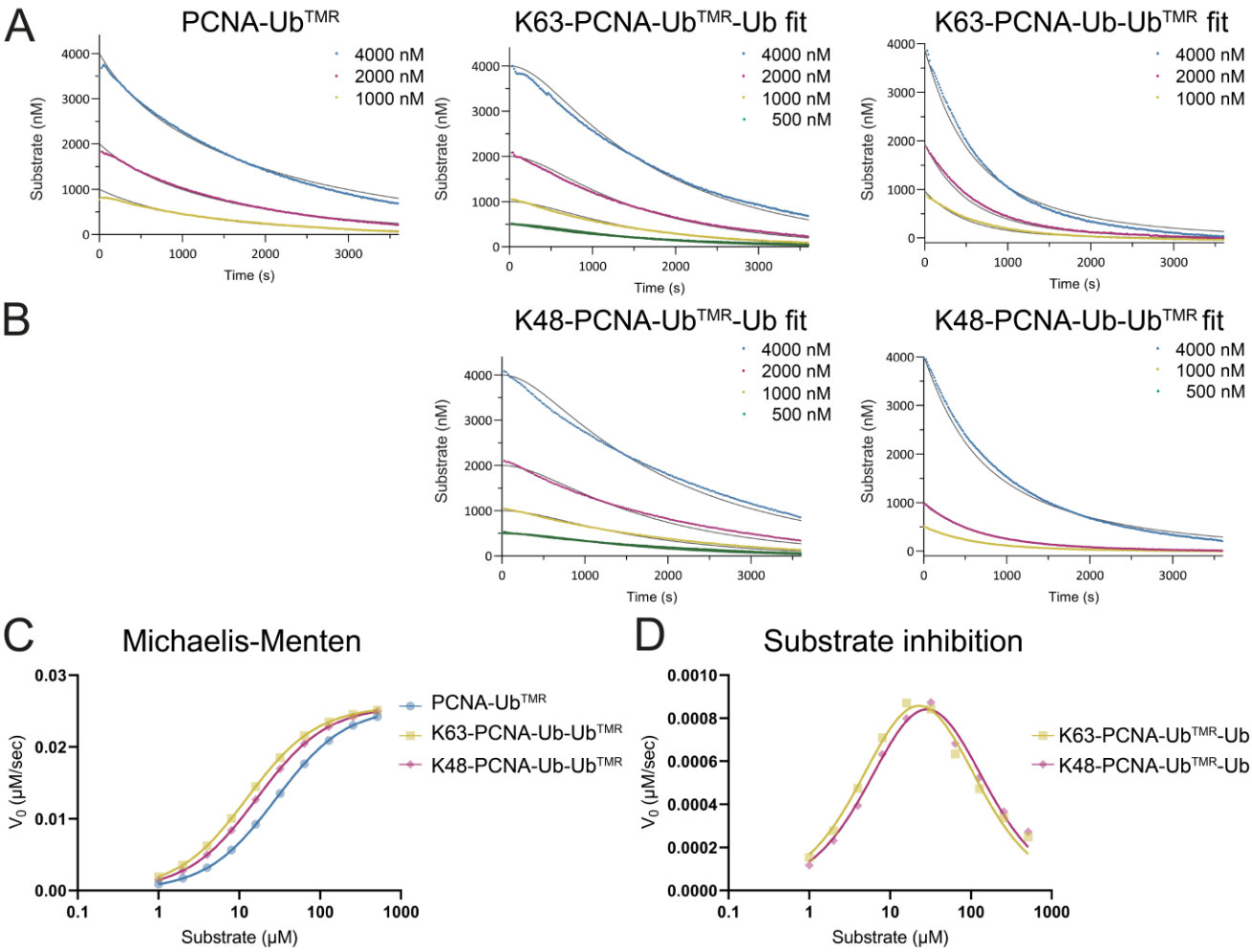

Supplementary figure 5 – Output of kinetic model

A) Kinetic fits generated using the kinetic model for K63 substrates (grey lines) plotted against FP data shown in supplementary figure 2 (dots). **B)** Kinetic fits generated using Kintek model for K48 substrates (grey lines) plotted against experimental data (dots). For both substrates, 2000 nM data was excluded from the kinetic model. **C)** Michaelis-Menten analysis of distally labeled K63- and K48-PCNA-Ub_2 and PCNA-Ub^{TMR} using data from the kinetic model. **D)** Substrate inhibition analysis of proximally labeled K63- and K48-PCNA-Ub_2 used to calculate reaction rates, using data from the kinetic model.

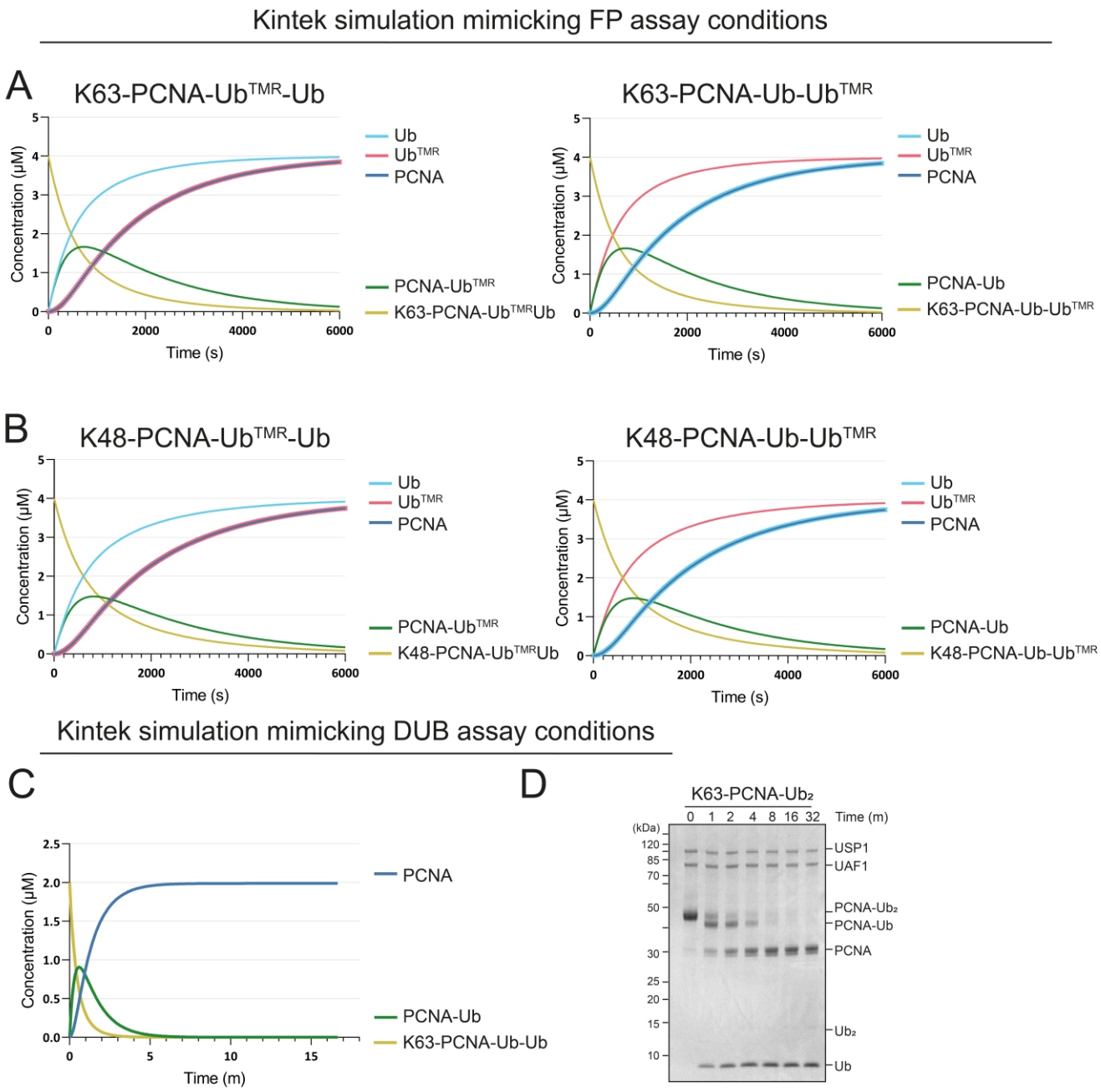

Supplementary figure 6 – KinTek model simulations reflect experimental observations

A) Simulation by kinetic model for K63-PCNA-Ub^{TMR}-Ub (same as in Fig. 3C) and K63-PCNA-Ub-Ub^{TMR} shows cleavage of substrates and appearance of different products as USP1/UAF1 cleaves PCNA-Ub$_2$. These simulations were performed for the enzyme and substrate concentrations of the FP assays in Figure 3A (USP1/UAF1: 10 nM, K63-PCNA-Ub$_2$: 4 µM). **B)** Same as in E) but for K48-PCNA-Ub^{TMR}-Ub and K48-PCNA-Ub-Ub^{TMR}. **C)** Kintek simulation mirroring the assay in figure 2E on K63-PCNA-Ub$_2$ (right panel, from Fig. 1E, USP1/UAF1: 200 nM, K63-PCNA-Ub$_2$: 2 µM) which demonstrates that the simulation fits the SDS page DUB assay using K63-PCNA-Ub$_2$ (shown in **(D),** same as in Fig. 2E). Simulation is shown for 16 minutes and not 32 minutes to make it easier to follow the PCNA-Ub curve.

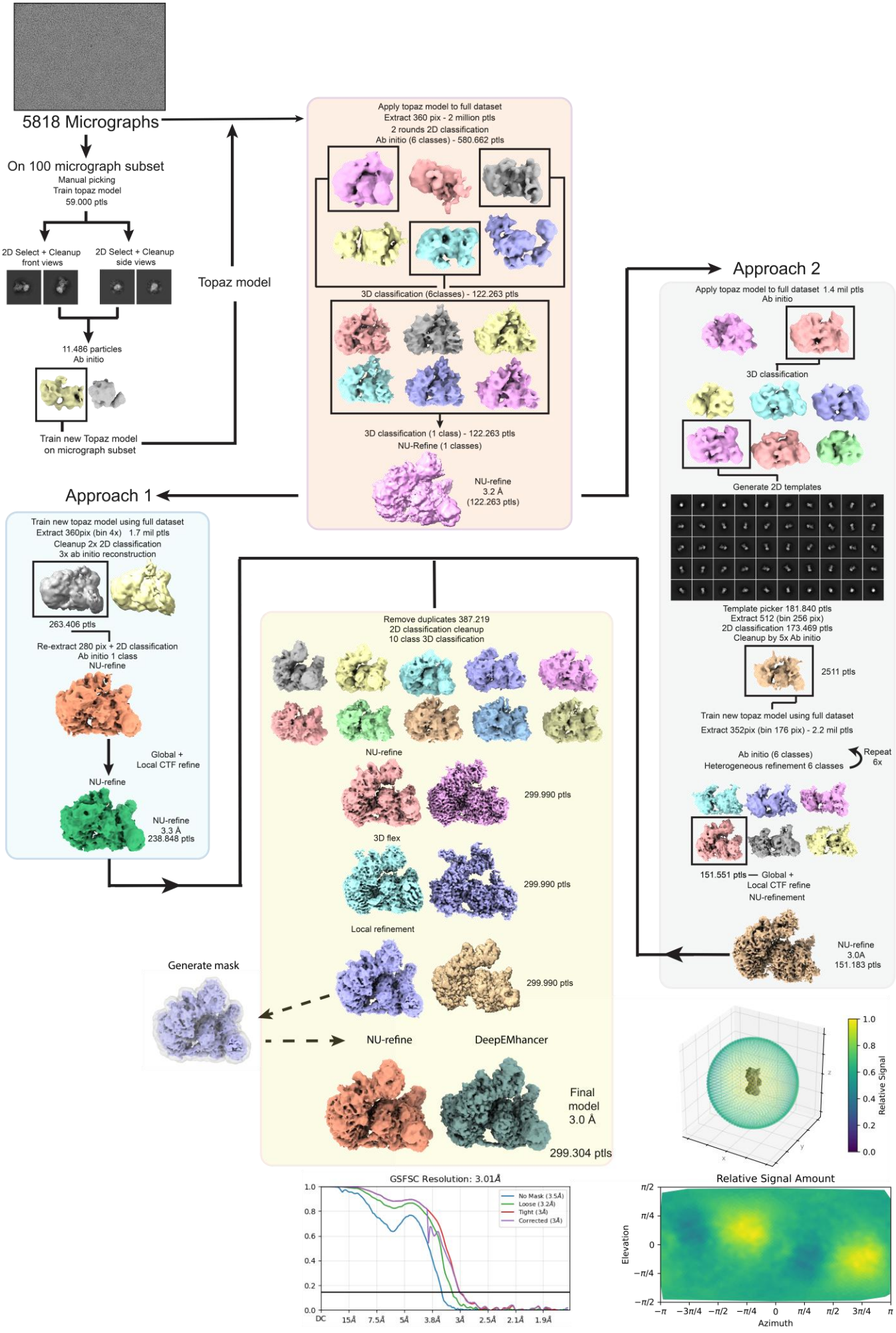

Supplementary figure 7 – Cryo-EM data processing workflow

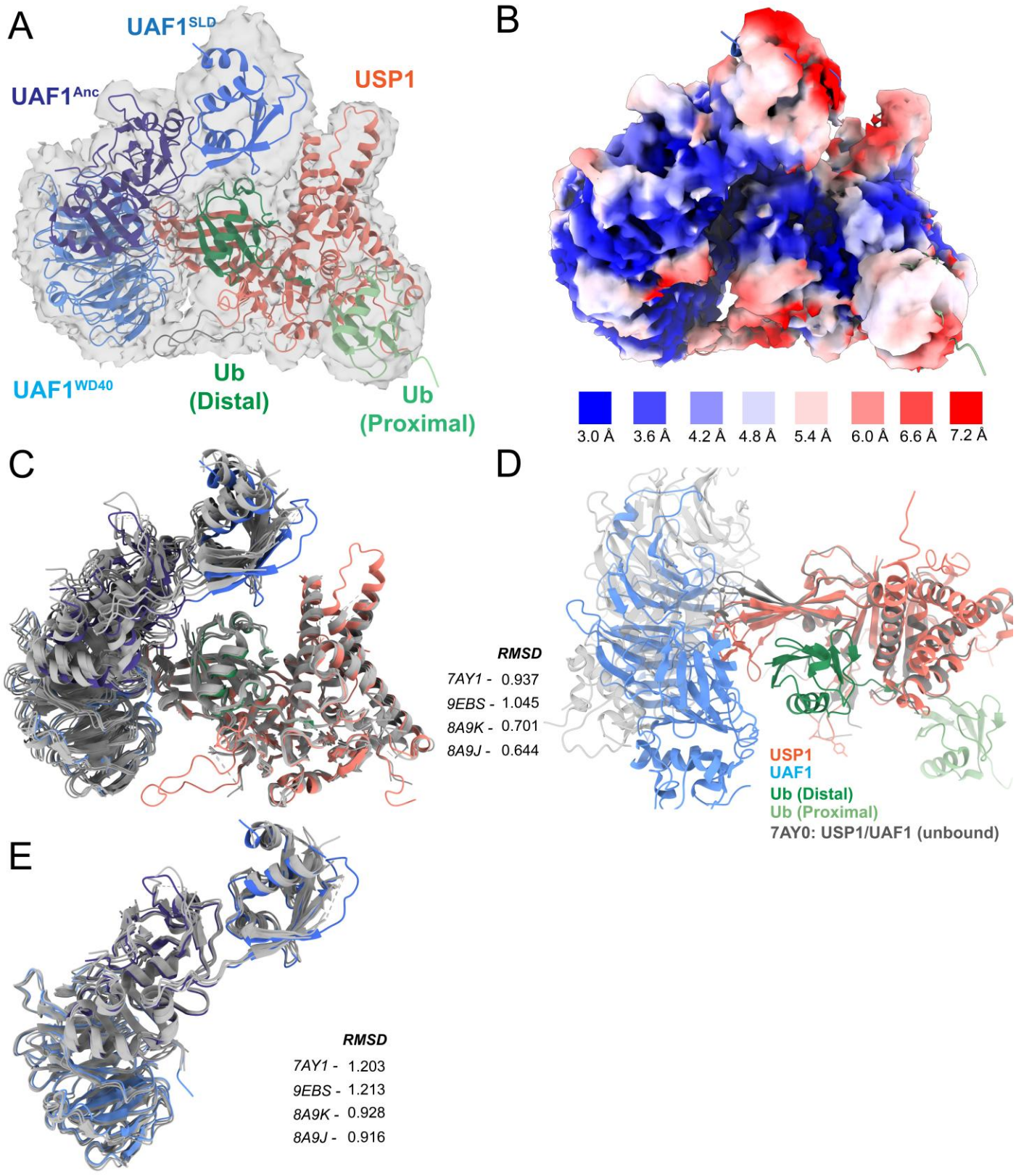

Supplementary figure 8 – Conformation of USP1/UAF1 bound to K63-Ub_2 resembles other USP1 structures

A) Atomic reconstruction of USP1/UAF1 bound to K63-linked $Ub_{VA}Ub$ probe, in density of the non-sharpened map, shown at threshold 0.015 to accentuate density for flexible regions. **B)** Local resolution image of the non-sharpened map of our structure shown at threshold 0.024. **C)** Structural superposition of USP1/UAF1 + K63-Ub_2 (coloured, proximal ubiquitin not shown), aligning USP1 to other experimental structures (7AYO, 8A9K, 8A9J, 9EBS (Rennie et al., 2021, 2022; Simoneau et al., 2025)), shown in grey. Our structure resembles other USP1 structures, with most variety observed in relative positioning UAF1's Ancillary and SLD-domains. RMSDs of the superposition to USP1 are shown. **D)** Structural superposition of USP1/UAF1 + K63-Ub_2 (coloured) to the crystal structure of the USP1/UAF1 apo-structure (7AY0 (Rennie et al., 2021)). **E)** Structural superposition of the same structures used in C, aligning to UAF1 instead (USP1 and Ub not shown) demonstrates that the structure of UAF1 itself does not deviate, but that it is its positioning towards USP1 that slightly varies. RMSDs of the superposition to UAF1 are shown.

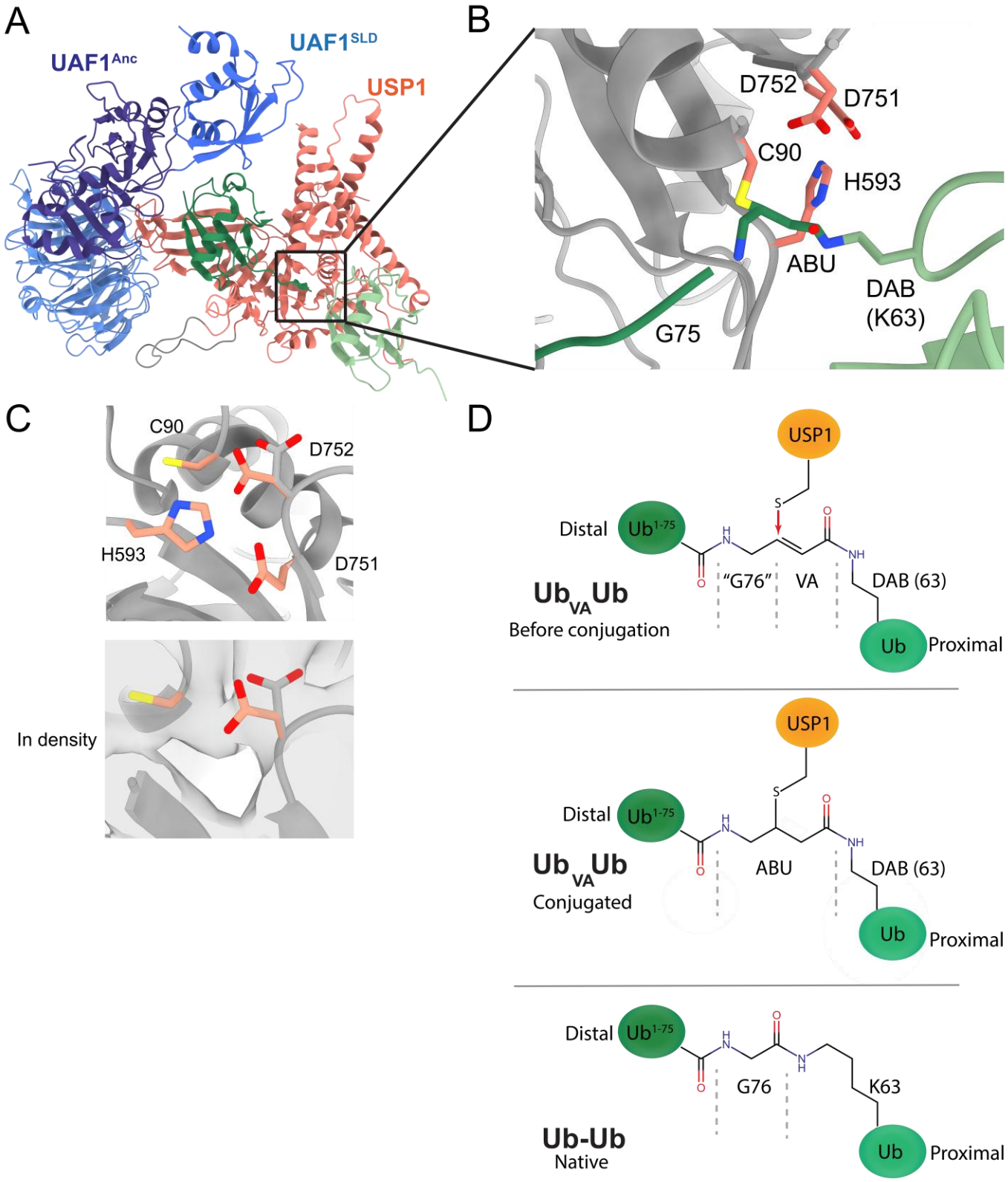

Supplementary figure 9 – Positioning of the activity-based probe in the USP1 active site

A) Structure of USP1/UAF1 covalently bound to K63-Ub$_{VA}$Ub. **B)** Zoom on the USP1 active site, showing catalytic C90 covalently bound to the activity-based probe, forming a 4-aminobutyric acid (ABU) linker (dark green); the ABU linker now connects G75 of the distal ubiquitin (dark green) with a 2,4-diaminobutyric acid residue (DAB) at position 63 of the proximal ubiquitin (light green) (see D). Catalytic residues C90, H593 and D751 and D752 are highlighted. **C)** D752 is essential for catalysis in USP1 (Keijzer et al,. 2024), but the density (lower panel) surrounding this residue allows for two different rotamers. We followed the canonical positioning (pink) in the deposited coordinates. **D)** Schematic of the K63-Ub$_{VA}$Ub linkage before and after conjugation to USP1's C90. As shown in the bottom panel, the K63-Ub$_{VA}$Ub linkage mimics the native isopeptide linkage between G76 of the distal ubiquitin and K63 of the proximal ubiquitin**.** Schematics were made using Marvin JS by Chemaxon.

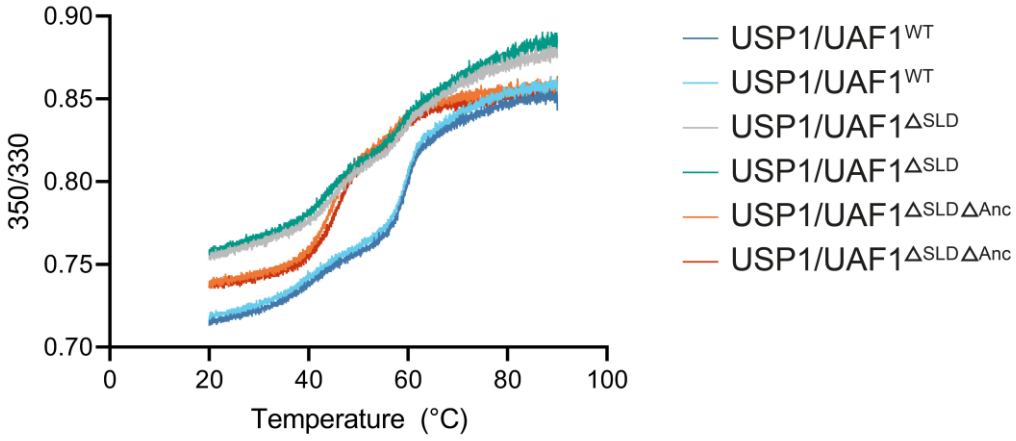

Supplementary figure 10 – Stability of UAF1 deletion mutants is comparible to UAF1^{WT}

Thermal stability analysis of UAF1 variants only shows a slight difference in melting temperature compared with UAF1^{WT}. Inflection points are shown in Supplementary table 3.

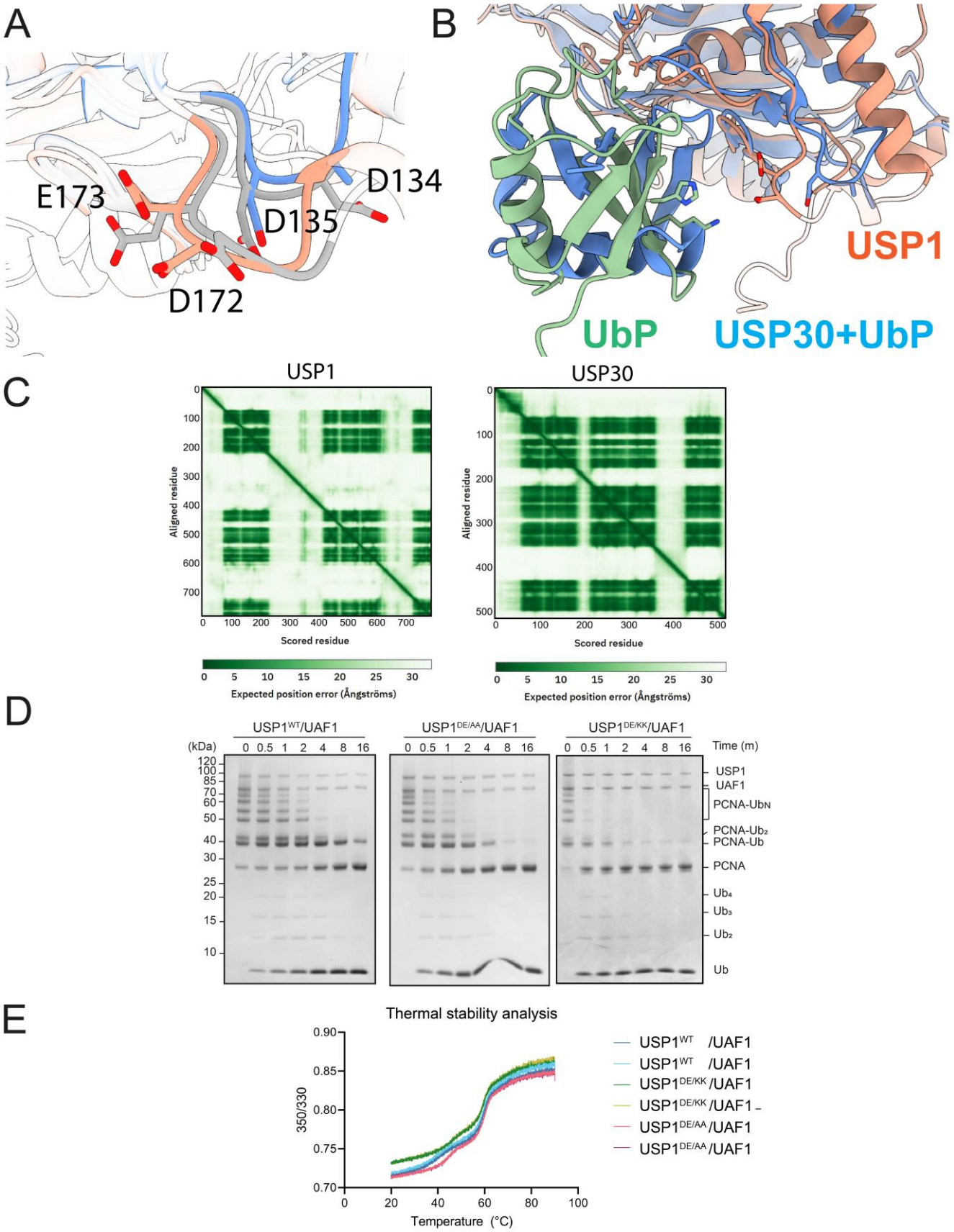

Supplementary figure 11 – Hyperactivation of USP1/UAF1 by mutating a conserved negative patch

A) Superposition of D172/E173 loop of USP1/UAF1, compared with equivalent loop in USP30 and their AlphaFold2 predictions shows that the loop is correctly predicted. Other human USPs do not have this loop, and are therefore not shown. Structure solved in this paper is solved in pink, superposed on USP1 AlphaFold2 prediction (grey). USP30 (5OHP (Gersch et al., 2017)) shown in blue with its AlphaFold2 prediction in grey. **B)** Superposition of USP1 and USP30 (5OHP) showing interface with the proximal ubiquitin. The D172/E173 equivalent residues in USP30 (D134/D135) are positioned further from the proximal ubiquitin. More importantly, since USP30 binds a K6-linked diubiquitin chain and as such the proximal ubiquitin is positioned different from how USP1 interacts the K63 proximal ubiquitin. **C)** PAE plots of USP1 and USP30 AlphaFold2 predictions. **D)** DUB assay on K63-PCNA-Ub_N comparing $USP1^{WT}$/UAF1, $USP1^{DE/AA}$/UAF1 $USP1^{DE/KK}$/UAF1. Mutating D172 and E173 causes hyper-activation of USP1 and does not change its cleavage mechanism. Uncropped gels are provided as source data. **E)** Thermal stability assay on $USP1^{D172/E173}$/UAF1 variants. $USP1^{DE/KK}$ and $USP1^{DE/AA}$ have higher thermal stability compared with $USP1^{WT}$. Inflection points are shown in Table S3.

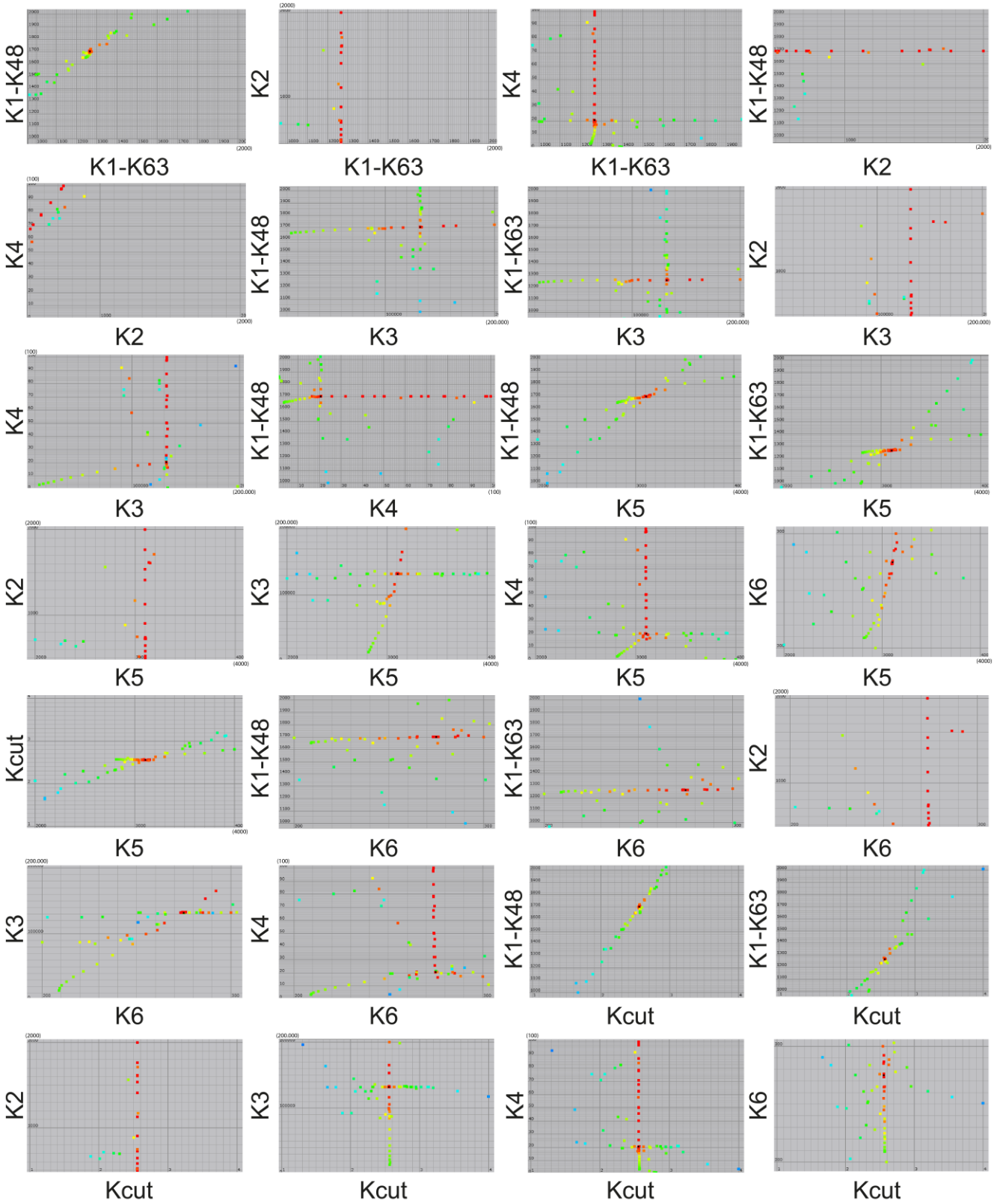

Supplementary figure 12 – Statistical analysis of Kinetic model

The Kintek FitSpace analysis visualizes model parameters through plots derived from 1D FitSpace calculations. These plots use a false-colour scale to represent normalized χ^2 values (scale is from 0 to 1, colours from green to red), highlighting the relationship between pairs of parameters. Many plots show strong overlap of the maximum values for both parameters (for example k5 vs k3, k5 vs kcut), indicating that these parameters are well-constrained and have defined maximum. Conversely, some plots reveal that the maximum value of one parameter is independent of the other (for example kcut vs k4, k5 vs k2), suggesting that these parameters do not directly influence each other.

Supplementary table 1 - Kinetic model and parameters/constants

Constants describing the different reactions and equilibriums in the kinetic models. kon is diffusion limited and therefore the same for each reaction. k1, k2, k3, k4, k5, k6 are the off rates for each reaction and can be seen as representations of affinity in this model. Initially, the kinetic constants for each K63- or K48-specific step were defined as independent, except the cleavage constant (kon and kcut). However, after fitting we realized that all constants for both linkages, except for k1, are similar, and thus were shared in the subsequent fitting steps. Additionally, dissociation rates of PCNA_USP1_Ub and PCNA_USP1 were originally independent from each other, but appeared to be similar and were defined as a single constant (k6) to describe both. Lower and upper boundaries shown for 95% confidence interval.

$$USP1 + PCNA\_Ub\_Ub \underset{k_1}{\overset{k_{on}}{\rightleftharpoons}} PCNA\_Ub\_Ub\_USP1 \xrightarrow{k_{cut}} PCNA\_Ub\_USP1\_Ub \underset{k_{on}}{\overset{k_2}{\rightleftharpoons}} PCNA\_Ub + USP1\_Ub \underset{k_{on}}{\overset{k_3}{\rightleftharpoons}} USP1 + Ub$$

$$PCNA\_Ub\_Ub\_USP1 \xrightarrow{k_4} PCNA\_Ub\_USP1 + Ub$$

$$USP1 + PCNA\_Ub \underset{k_5}{\overset{k_{on}}{\rightleftharpoons}} PCNA\_Ub\_USP1 \xrightarrow{k_{cut}} PCNA\_USP1\_Ub \underset{k_{on}}{\overset{k_6}{\rightleftharpoons}} PCNA + USP1\_Ub \underset{k_{on}}{\overset{k_3}{\rightleftharpoons}} USP1 + Ub$$

$$USP1 + PCNA \underset{k_6}{\overset{k_{on}}{\rightleftharpoons}} PCNA\_USP1$$

K63 kinetic model				
Parameter	**Best fit**	**Standard Error**	**Lower Bound**	**Upper Bound**
k_{on} ($\mu M^{-1}*s^{-1}$)	100			
k_{cut} (s^{-1})	2.6	0.06	2.5	2.63
k_1 (s^{-1})	1244	8.5	1230	1350
k_2 (s^{-1})	932	554	200	2280
k_3 (s^{-1})	3840	485	3000	10000
k_4 (s^{-1})	5.5	3	3	56
k_5 (s^{-1})	2812	60	2700	3300
k_6 (s^{-1})	229	6.7	225	310

K48 kinetic model				
Parameter	**Best fit**	**Standard Error**	**Lower Bound**	**Upper Bound**
k_{on} ($\mu M^{-1}*s^{-1}$)	100			
k_{cut} (s^{-1})	2.6	0.06	2.5	2.63
k_1 (s^{-1})	1656	8.9	1650	1760
k_2 (s^{-1})	932	554	200	2280
k_3 (s^{-1})	3840	485	3000	10000
k_4 (s^{-1})	5.5	3	3	56
k_5 (s^{-1})	2812	60	2700	3300
k_6 (s^{-1})	229	6.7	225	310

Supplementary table 2 – Cryo-EM data collection and refinement statistics

Data collection and processing	**EMD:** 52316
Magnification	105.000x
Voltage (kV)	300
Electron exposure (e–/Å^2)	50
Defocus range (μm)	-1.2, -2.4
Pixel size (Å)	0.836
Symmetry imposed	C1
Initial particle images (no.)	3.110.350
Final particle images (no.)	299.304
Map resolution (Å) FSC threshold	3.01 0.143
Map sharpening *B* factor (Å^2)	DeepEMhancer
Refinement	**PDB:** 9NHW
Initial model used (PDB code)	Alphafold2 1UBQ
Model resolution (Å) FSC threshold	3.47 0.143
Model composition Non-hydrogen atoms Protein residues Ligands	 9350 1180 3
B factors (Å^2) Protein	 116
R.m.s. deviations Bond lengths (Å) Bond angles (°)	 0.004 (3) 0.555 (2)
Validation MolProbity score Clashscore Poor rotamers (%)	 1.73 9.43 0.19
Ramachandran plot Favored (%) Allowed (%) Disallowed (%)	 96.57 3.43 0.00

Supplementary table 3 – Thermal stability of USP1/UAF1 mutants.

Inflection points of USP1/UAF1 variants measured using microscale thermophoresis. USP1/UAF1 has two inflection points for USP1 (#1) and UAF1 (#2). Interestingly, double mutants of $USP1^{D172/E173}$ causes an increase in thermal stability. Deletions of UAF1 only cause minor decrease in thermal stability.

	Inflection point #1 (USP1)	Inflection point #2 (UAF1)
$USP1^{wt}$ /UAF1	41.8 °C	59.7 °C
$USP1^{wt}$ /UAF1	42.9 °C	59.3 °C
$USP1^{DE/KK}$/UAF1	46.3 °C	59.5 °C
$USP1^{DE/KK}$/UAF1	46.4 °C	59.5 °C
$USP1^{DE/AA}$/UAF1	44.03 °C	60.1 °C
$USP1^{DE/AA}$/UAF1	45.1 °C	60.2 °C
$USP1^{WT}$ /$UAF1^{\Delta SLD}$	44.8 °C	59.3 °C
$USP1^{WT}$ /$UAF1^{\Delta SLD}$	44.2 °C	58.5 °C
$USP1^{WT}$ /$UAF1^{\Delta ANC+SLD}$	44.7 °C	57.1 °C
$USP1^{WT}$ /$UAF1^{\Delta ANC+SLD}$	45.8 °C	58.5 °C

Supplementary References

Keijzer, N., Priyanka, A., Stijf-Bultsma, Y., Fish, A., Gersch, M., & Sixma, T. K. (2024). Variety in the USP deubiquitinase catalytic mechanism. Life Science Alliance, 7(4). https://doi.org/10.26508/LSA.202302533

Rennie, M. L., Arkinson, C., Chaugule, V. K., Toth, R., & Walden, H. (2021). Structural basis of FANCD2 deubiquitination by USP1−UAF1. Nature Structural and Molecular Biology, 28(4), 356–364. https://doi.org/10.1038/s41594-021-00576-8

Rennie, M. L., Arkinson, C., Chaugule, V. K., & Walden, H. (2022). Cryo-EM reveals a mechanism of USP1 inhibition through a cryptic binding site. Science Advances, 8(39), 6353. https://doi.org/10.1126/SCIADV.ABQ6353

Simoneau, A., Pratt, C. B., Wu, H.-J., Rajeswaran, S. S., Comer, C. G., Sudsakorn, S., Zhang, W., Liu, S., Meier, S. R., Choi, A. H., Khendu, T., Stowe, H., Shen, B., Whittington, D. A., Chen, Y., Yu, Y., Mallender, W. D., Feng, T., Andersen, J. N., … Throner, S. (2025). Characterization of TNG348: A Selective, Allosteric USP1 Inhibitor That Synergizes with PARP Inhibitors in Tumors with Homologous Recombination Deficiency. Molecular Cancer Therapeutics, OF1–OF14. https://doi.org/10.1158/1535-7163.MCT-24-0515